

Original Research

Geochemical Evolution of Antimony Content in Shallow Groundwater After Ecological Restoration Project in Xikuangshan, Hunan Province, China

Ximeng Sun¹, Yantang Wang¹, Kaikai He¹, Min Liu¹, Yingao Peng², Chunming Hao^{1,3*}

¹North China Institute of Science and Technology, Hebei, 065201, P.R. China

²Institute of Disaster Prevention, Hebei, 065201, P.R. China

³Observation and Research Station of Lengshuijiang Mining Ecological Environmental Monitoring, Ministry of Natural Resources, Changsha, Hunan 410004, China

Received: 22 May 2023

Accepted: 8 July 2023

Abstract

The ecological restoration project of Xikuangshan (XKS) effectively reduces environmental pollution. However, the hydrogeochemical factors and mechanisms leading to the evolution of antimony (Sb) content in shallow groundwater after ecological restoration have not been studied. In order to investigate the geochemical evolution of Sb content in shallow groundwater, 64 samples were collected before and after the ecological restoration project. The results showed Sb concentrations in shallow groundwater before and after ecological restoration were 0.006-39.160 mg/L (mean 3.501 mg/L), and 0.003-17.326 mg/L (mean 2.931 mg/L), respectively. The high Sb content before ecological restoration was mainly caused by the oxidation of Sb_2S_3 , dissolution of carbonate and silicate minerals, evaporation/concentration effects, and cation exchange. The weaker oxidation of Sb_2S_3 and effective cleaning of the arsenic alkali residue reduced the Sb content in shallow groundwater after ecological restoration. This study provides a basis for understanding the effects of ecological restoration projects on the evolution of Sb content in shallow groundwater, and provides a new idea for solving groundwater pollution and promoting groundwater resources management.

Keywords: antimony, ecological restoration, hydrogeochemistry, evolution

Introduction

Antimony (Sb) is a metalloid with a metallic luster, that mainly exists in the lithosphere as stibnite (Sb_2S_3) and diantimony trioxide (Sb_2O_3). Sb and its compounds are widely used for the production of fire retardants, alloys, and semiconductor materials [1-3]. Sb is potentially toxic and carcinogenic to humans, causing damage to the immune and nervous systems [4-6]. Therefore, it is considered a priority pollutant by the European Union (EU) and the United States Environmental Protection Agency (USEPA).

The problem of Sb pollution in the environment caused by mining activities and the extensive use of Sb in industry in recent years has gradually increased and attracted considerable attention worldwide [7-11]. The exploitation and smelting of Sb ores and random stacking of Sb-containing tailings are believed to be among the main causes of Sb pollution in aquatic environments [10, 12-15]. Primary Sb minerals are usually sulfides because of the different affinities of Sb for sulfur and oxygen. The oxidative dissolution of Sb-containing sulfides is the main mechanism by which Sb enters the aquatic environment [16-18]. Mining activities expose Sb minerals to an oxidizing environment, releasing the heavy metal Sb from minerals into the aquatic environment. Water pollution caused by Sb occurs frequently worldwide [9, 19, 20]. The concentration of Sb in the surface water downstream from the mine in Sardinia, Italy, was as high as 1500 $\mu\text{g/L}$, and in the river water flowing 200m downstream of the mine area reached 28 $\mu\text{g/L}$. The mine and tailings dam water at Hillgrove, New South Wales, contained up to 55 mg/L dissolved Sb, and the stream immediately downstream from the mine contained 1.8 mg/L. In China, the Sb content in the Banpo Sb mining area of Guizhou Province is as high as 1377 $\mu\text{g/L}$ [7, 8, 21, 22].

China was one of the first countries to discover and utilize Sb worldwide. According to data from the U.S. Geological Survey in 2020, the proven reserves of Sb in the world in 2019 were 1.5 million tons, and the reserves of Sb in China reached 480,000 tons, accounting for 32% of the total reserves of Sb in the world [23, 24]. Most Sb and its compounds are produced in Xikuangshan (XKS), Hunan Province, which is known as the "World Capital of Antimony". Long-term irrational mining of Sb in the XKS produces a large amount of solid waste. Most of the arsenic alkali residue produced by Sb smelting is not properly handled, resulting in the discharge of Sb-containing pollutants into groundwater and excessive Sb content in the water environment [1, 25]. The study showed that the content of Sb in the water environment of Hunan Sb mine was 29423 $\mu\text{g/L}$, which was 5884 times higher than the standards for drinking water (GB5749-2022) [26]. High Sb content seriously threatens the safety of drinking water for residents. To control the discharge of Sb-containing pollutants effectively, a local ecological restoration project was

initiated in 2016. By improving waste solid treatment and plant remediation, XKS mine area has reduced the discharge of wastewater and arsenic alkali residue and promoted local environment quality. Meanwhile, the highest content of Sb in the groundwater samples collected from XKS after ecological restoration project was 7450 $\mu\text{g/L}$, which was significantly lower than that before ecological restoration project [27]. Currently, research on the changes and mechanisms of Sb content in shallow groundwater before and after ecological restoration is lacking. The study of Sb content evolution before and after the ecological restoration project is of great significance in understanding the impact of anthropogenic activities on shallow groundwater, and improving groundwater environment in XKS mine area.

Accordingly, hydrogeochemical data of shallow groundwater before and after ecological restoration were collected with the following aims: (1) to understand the evolution of hydrogeochemical ions before and after ecological restoration; (2) to assess the hydrogeochemical factors that contribute to the high level of Sb in shallow groundwater; and (3) to determine the formation mechanism of high Sb content in shallow groundwater before and after ecological restoration.

Study Area

The XKS Sb mine is located at $111^{\circ}25'47''$ - $111^{\circ}31'22''$ east and $27^{\circ}49'28''$ - $27^{\circ}43'05''$ north, about 13 kilometers north of Lengshuijiang City, Hunan Province (Fig. 1). The main body of the mine is divided into southern and northern mines, and covers an area of 26 km^2 . The climate in the study area is subtropical monsoon, with average annual rainfall, evaporation, and annual temperature of 1381.6 mm, 903.3 mm, and 16.7°C, respectively. The area is dominated by seasonal streams such as the Batangshan, Xuanshan, Feishuiyan, and Tanjiachong streams, all of which belong to the Zijiang River system.

The XKS Sb mine is located in the South China antimony metallogenic belt, which is tectonically located at the intersection of the NE trending Taojiang-Chengbu deep great fault zone and the NW trending Xinhua-Lianyuan basement fault zone [28, 29]. The mining area is distributed along the XKS complex anticline. The western anticline is cut by the F_{75} fault, which is a part of the Taojiang-Chengbu deep fault, and the eastern anticline is cut by the lamprophyre vein.

The main exposed formations in the mining area are the Shetianqiao (D_3s) and Xikuangshan formations (D_3x). The main aquifers are the fractured karst aquifer in Magunao in the Xikuangshan formation (D_3x^4) and the fractured karst aquifer in the limestone section of the Shetianqiao formation (D_3s^2) [2]. The D_3x^4 aquifer is mainly composed of limestone and sandy limestone with a thickness of 258 m and an average permeability coefficient of 0.0092 m/d. Several exposed springs with

flow rate of 0.1-0.7L/S. The D_3s^2 aquifer is composed of mica limestone, silicified limestone, and shale, with a thickness of approximately 220 m. The average water conductivity was 0.041 m/d and contained an Sb ore-body, which was significantly affected by mining activities. The aquifer is mainly charged by atmospheric precipitation and drains mainly through springs. Regional groundwater mainly flows from southeast to northwest in the northern mine, whereas that of the southern mine moves from northeast to southwest [30].

Sample Collection and Analysis

Sample Collection

In order to evaluate the evolution of Sb content before and after ecological restoration project in shallow groundwater, 64 samples were collected in this study, including 25 before and 39 after ecological restoration (Fig. 1). Water samples were filtered through 0.45 μm millipore filters and collected in high-density polyethylene (HDPE) bottles. Before collection, the sampling bottles were washed two or three times with distilled water and then washed two to three times with sample water. At each sampling site, three bottles of 500 ml water were collected. One bottle was the original sample, and one bottle was acidified to $\text{pH} < 2$ with 1:1 (v/v) nitric acid, which was used

for the determination of cations and trace elements, and 0.25 mol/L ethylenediamine tetraacetic acid (EDTA) and hydrochloric acid solution were added to the third bottle of water for the subsequent determination of the valence states [31, 32]. All samples were refrigerated at 4°C before being sent to the laboratory for analysis, and most indicators were analyzed and determined by the Hunan Geological Experiment and Testing Center.

Sample Analysis

The pH and total dissolved solids (TDS) were measured on-site using portable pH (HANNA H18424) and conductivity meters (HANNA H1833), respectively. The main cations (K^+ , Ca^{2+} , Na^+ , and Mg^{2+}) were measured by inductively coupled plasma Atomic emission spectrometer (ICP-AES) with a detection limit of 0.01 mg/L, whereas the main anions (Cl^- , SO_4^{2-} , and NO_3^-) were measured by ion chromatograph (Dionex ICS-1100) with the analytical accuracy of 0.01 mg/L, and anion HCO_3^- was measured by titration with the analytical accuracy of 0.1 mg/L. The Sb concentration was measured using an atomic fluorescence spectrometer (AFS-830a) with an accuracy of 0.001 mg/L.

Analytical Quality Control

To ensure the accuracy and precision of the analysis results, each group of experiments included a blank

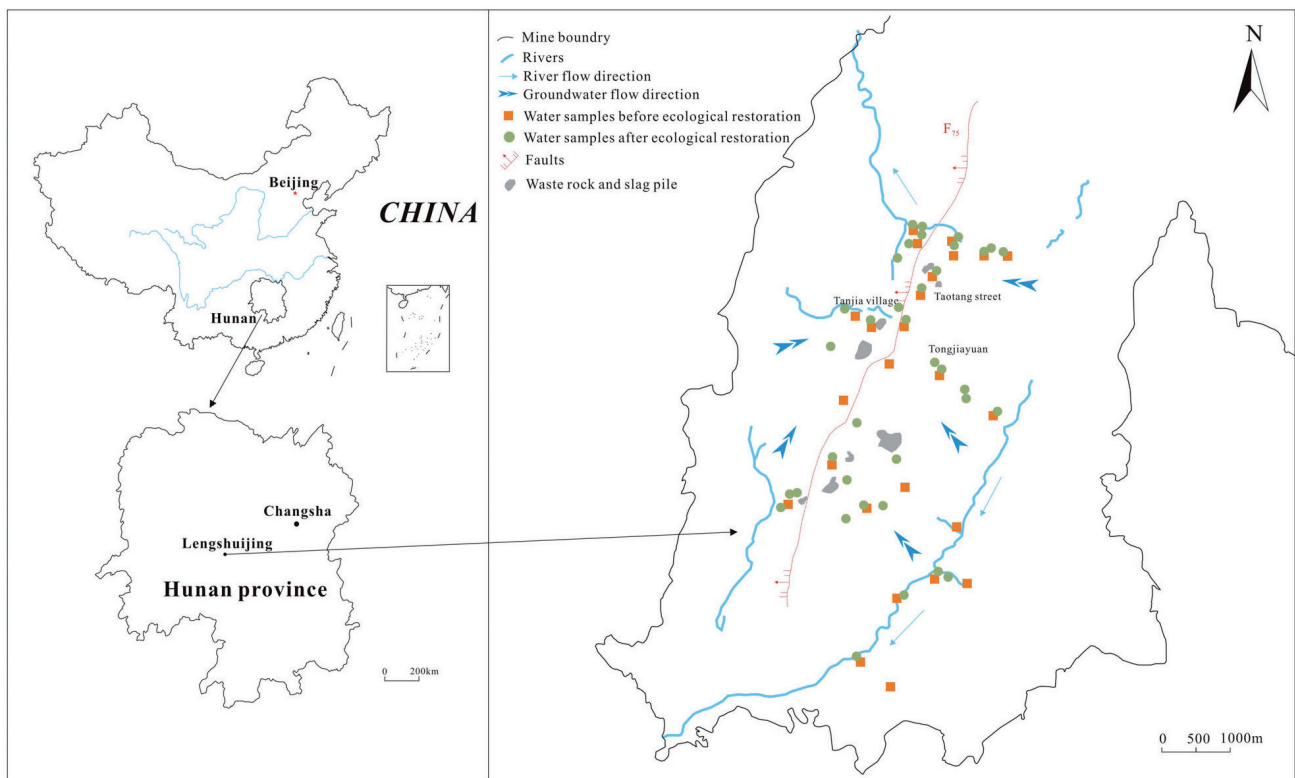


Fig. 1. Locations of the study area and samples collected in this study.

experiment to eliminate the influence of high blank values. Three sets of parallel samples were used, and each reported value was the average of the three tests to reduce random errors. The relative standard deviation was within 10%, and the recovery rate of standard addition was guaranteed to be 90-100%. 20% of the samples submitted for analysis were blinded, and the absolute ion balance error of the water chemical ions was less than 5%.

Statistical Analysis

Origin 2022 software was used to perform descriptive statistical analysis. Piper diagram was used to elucidate the hydrogeochemical facies. The PHREEQC geochemical model was used to calculate the saturation indices (SI) to assess whether the mineral is saturated.

Results

Hydrogeochemical Characteristics of Shallow Groundwater

The geochemical characteristics of the shallow groundwater before and after ecological restoration in the study area are shown in Table 1. The pH values before and after ecological restoration were 6.04-7.70 (mean 7.20) and 4.97-9.32 (mean 7.13), respectively. The shallow groundwater samples were weakly alkaline, which was consistent with the results of a previous study [30]. The TDS values ranged from 210 to 1156 mg/L (mean 428 mg/L) before ecological restoration. The TDS values after ecological restoration ranged from 135 to 1311 mg/L, with an average of 504 mg/L, which was higher than the mean value of TDS before ecological restoration, indicating that the ecological restoration process strengthened the water-

rock action in shallow groundwater [2, 33]. In addition, 4.00% of the shallow groundwater samples before the ecological restoration and 10.26% of the shallow groundwater samples after the ecological restoration had TDS values above 1000 mg/L, which exceeded the standards for drinking water (1,000 mg/L; GB5749-2022).

Ca²⁺ was the main cation in shallow groundwater before ecological restoration, accounting for 68.54% of the total cations, followed by Na⁺, and the main hydrochemical types were Ca-Na-SO₄-HCO₃ (36.00%), Ca-HCO₃-SO₄ (32.00%), and Ca-SO₄-HCO₃ (16.00%) (Fig. 2). Ca²⁺ and Na⁺ were the main cations present after ecological restoration. The mean Na⁺ increased by 1.32 times compared to that before ecological restoration. The hydrochemical types were Ca-HCO₃-SO₄ (33.33%), Ca-SO₄-HCO₃ (33.33%), and Ca-Na-SO₄-HCO₃ (12.82%) (Fig. 2).

SO₄²⁻ was the predominant anion before the ecological restoration, with an average concentration of 165.62 mg/L. The mean SO₄²⁻ content after ecological restoration (247.94 mg/L) was higher than that before restoration. Before and after ecological restoration, HCO₃⁻ was the second highest anion content, ranging from 6.1-230.4 mg/L (mean 116.3 mg/L) and 9.2-600.0 mg/L (mean 177.0 mg/L), respectively.

The Sb concentrations in shallow groundwater before and after ecological restoration were 0.006-39.160 mg/L (mean 3.501 mg/L), and 0.003-17.326 mg/L (mean 2.931 mg/L), respectively. The average Sb content after ecological restoration decreased by 0.57 mg/L compared with that before ecological restoration, indicating that ecological restoration could effectively reduce the concentration of Sb in groundwater. Moreover, the Sb contents before and after ecological restoration exceeded the value of the standards for drinking water (5 µg/L; GB5749-2022), and the exceeded multiple is 699 and 585 times, respectively.

Table 1. Geochemical data of samples collected in this study.

Types	Sb	K ⁺	Na ⁺	Ca ²⁺	Mg ²⁺	Cl ⁻	SO ₄ ²⁻	HCO ₃ ⁻	NO ₃ ⁻	TDS	pH
	mg/L										
Before ecological restoration (n = 25)											
Min	0.006	0.18	2.35	21.38	1.61	0.54	33.64	6.1	0.68	210	6.04
Max	39.160	8.02	108.13	225.17	57.49	47.68	707.70	230.4	57.52	1156	7.70
Mean	3.501	1.70	24.81	75.32	8.06	6.33	165.62	116.3	14.31	428	7.20
SD	8.354	1.83	26.95	44.89	11.51	10.25	149.04	52.2	15.89	247	0.32
After ecological restoration (n = 39)											
Min	0.003	0.18	0.04	14.00	1.58	0.30	47.10	9.2	0.02	135	4.97
Max	17.326	7.73	395.00	258.00	54.60	34.70	795.00	600.0	45.40	1311	9.32
Mean	2.931	2.85	32.94	84.20	10.83	4.74	247.94	177.0	8.62	504	7.13
SD	4.612	2.53	68.90	52.54	13.66	6.61	195.97	97.3	10.13	325	0.63

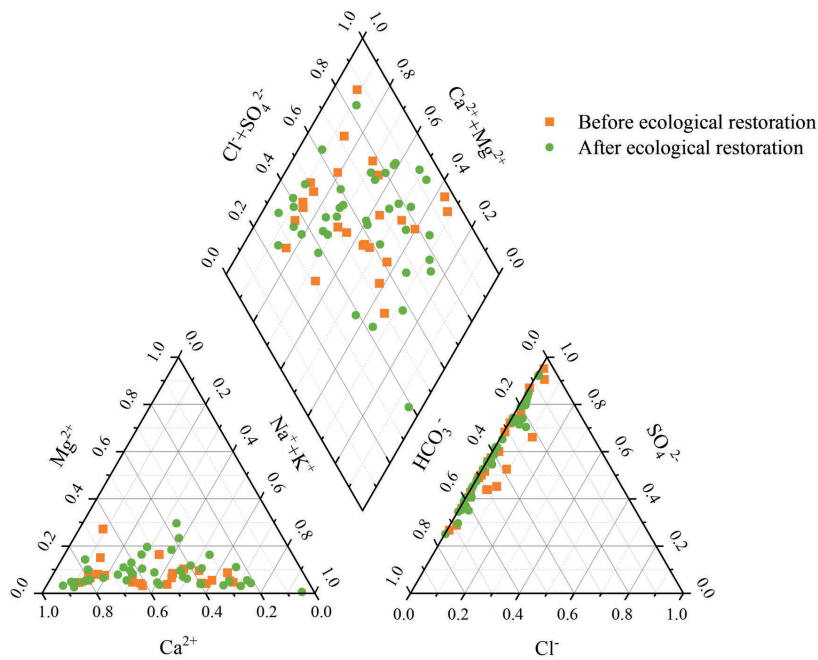


Fig. 2. Piper diagram of ionic composition of shallow groundwater samples.

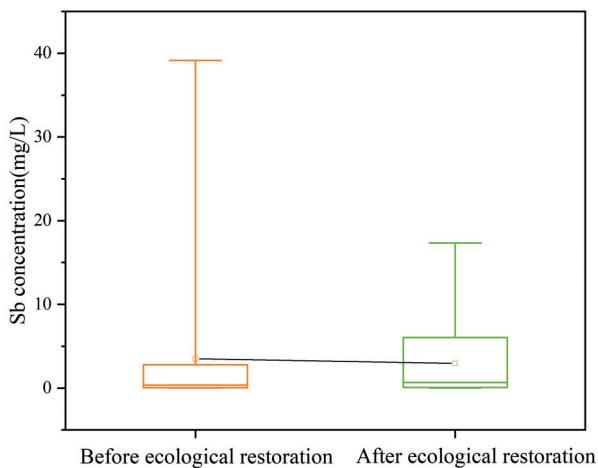


Fig. 3. Boxplots of variation in Sb concentration of shallow groundwater samples.

Characteristics of Interannual Variation of Typical Samples

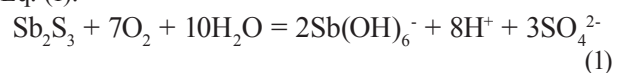
The interannual variation characteristics of Sb content were analyzed by selecting typical samples from historical waste rock and slag accumulation areas. As shown in Fig. 4a), the Sb content in shallow groundwater showed a downward trend. Before ecological restoration, the Sb content decreased, except for a slight increase in 2014. The Sb-containing wastewater infiltrated the shallow groundwater, resulting in an increase in Sb content [18]. The Sb content decreased after ecological restoration, which may be related to the ecological restoration projects.

The Ca^{2+} , Mg^{2+} , and K^+ contents exhibited a decreasing trend, whereas the Mg^{2+} and K^+ contents showed little variation. The variation range of the Na^+ content was wide, showing a trend of first decreasing, then increasing, then decreasing, and finally increasing (Fig. 4b). The content of Cl^- in the anions first decreased and then increased within a small range. The interannual changes in SO_4^{2-} and NO_3^- were similar, showing a trend of first increasing, then decreasing, and finally increasing again. The HCO_3^- content showed a trend of first decreasing and then increasing, followed by a decrease and then an increase. The SO_4^{2-} and HCO_3^- concentrations reached their highest levels in 2020 (Fig. 4c). The TDS content decreased from 2011 to 2015, and increased from 2016 to 2020 (Fig. 4d).

Discussion

Sb-Bearing Mineral Dissolution Before and After Ecological Restoration

Sb_2S_3 was the main Sb-bearing sulfide mineral in the XKS Sb mine [1, 2, 34]. Sb_2S_3 dissolves under oxidizing conditions during the mining process, as expressed in Eq. (1):



Based on Eq. (1), the Sb/SO_4^{2-} molar ratio was 2/3. As shown in Fig. 5a, before and after the ecological restoration, most of the water chemical samples were located on the right side of the Sb_2S_3 oxidation reaction line. The presence of excess SO_4^{2-} indicated that mining

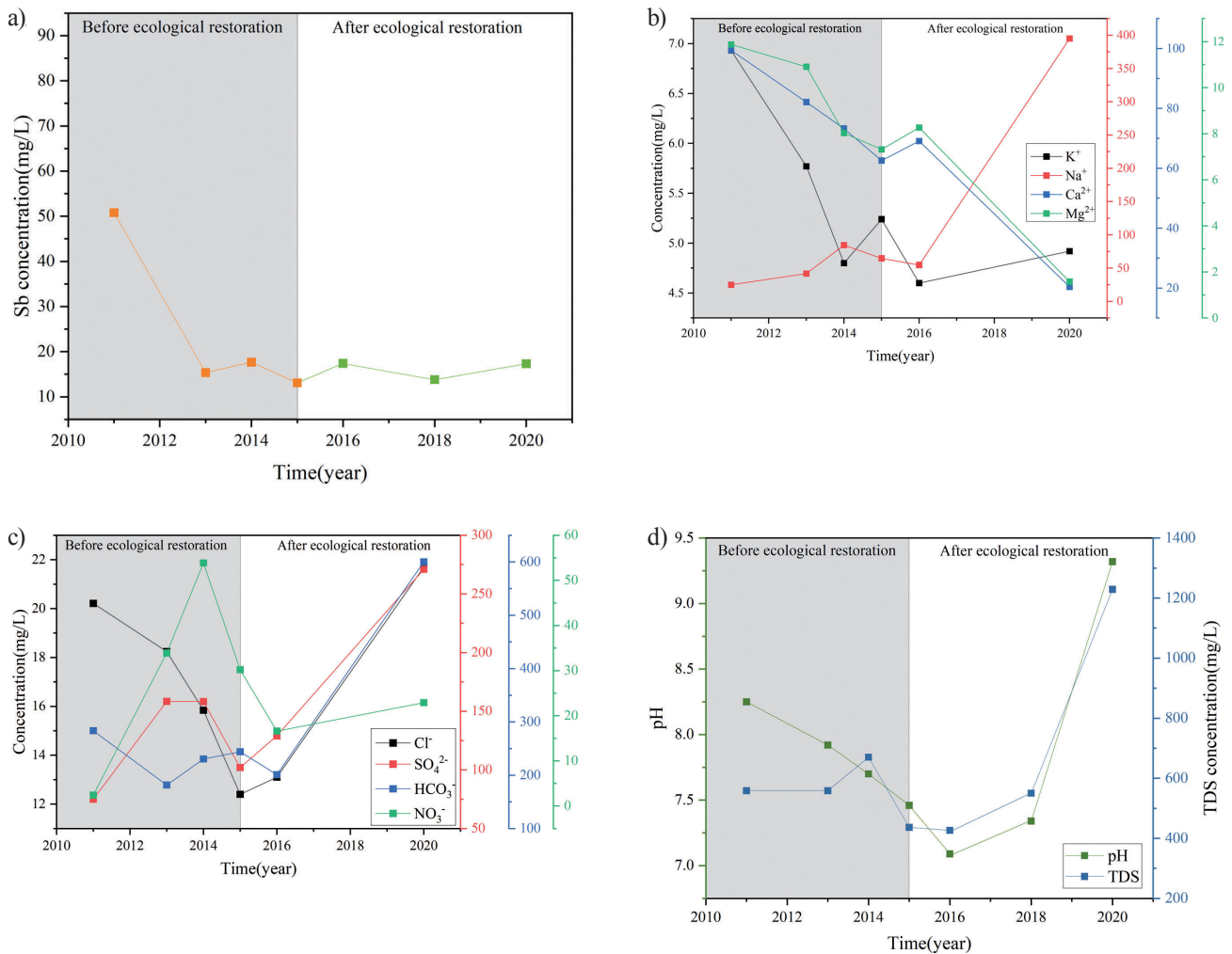


Fig. 4. Plots illustrating variations in a) Sb; b) K^+ , Na^+ , Ca^{2+} and Mg^{2+} ; c) Cl^- , SO_4^{2-} , HCO_3^- and NO_3^- ; d) pH and TDS in shallow groundwater during 2011–2020.

activities induced the dissolution of other sulfate-bearing minerals, including pyrite (FeS_2) [1, 28, 35]. Before and after the ecological restoration, some water samples had Sb/SO_4^{2-} molar ratios between 0.0008 and 0.016 (Fig. 5a), which were significantly lower than those of Sb/SO_4^{2-} dissolved by the oxidation of Sb_2S_3 , indicating that these water samples may have the same source of Sb/SO_4^{2-} [36].

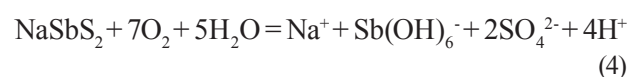
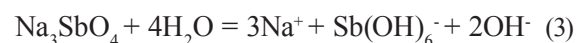
As the primary source mineral of Sb, Sb_2S_3 dissolves in water. When the SO_4^{2-} content increases, the Sb content decreases (Eq. (1)) [36]. Based on this mechanism, the main factors controlling gypsum ($CaSO_4$) weathering can be expressed as follows:

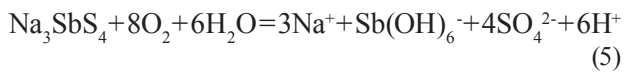


The dissolution of $CaSO_4$ will generate SO_4^{2-} , and the high SO_4^{2-} concentration may cause a left shift in the equilibrium of Eq. (1), which reduced the $Sb(OH)_6^-$. The saturation index (SI) indicates the ability of rock minerals to dissolve in groundwater. Fig. 6 shows the SIs of $CaSO_4$ and Sb_2S_3 in the shallow groundwater samples

[37]. 52% of the samples before ecological restoration and 28% of the samples after ecological restoration were unsaturated with respect to Sb_2S_3 ($SI < 0$), indicating that the oxidative dissolution of Sb_2S_3 would increase the Sb content in the water environment; however, the oxidative dissolution of Sb_2S_3 was weakened after ecological restoration. This is one of the reasons for the reduction in Sb content after ecological restoration. All the shallow groundwater samples were undersaturated with respect to $CaSO_4$ ($SI < 0$), indicating that the dissolution of $CaSO_4$ increased the SO_4^{2-} content and inhibited the dissolution of Sb_2S_3 , thereby reducing the Sb content.

Smelting in the Sb mine produces solid wastes, such as arsenic alkali residue, in which Sb mainly exists in the forms of Na_3SbO_4 , $NaSbS_2$, and Na_3SbS_4 [38, 39]. The equations used are as follows:





If arsenic alkali residue leaching occurs, Sb and Na⁺ exhibit a certain correlation. As shown in Fig. 5c), there was a positive correlation between Sb and Na⁺ after ecological restoration (R² = 0.42), and the correlation was higher than that before ecological restoration, indicating that the soil was disturbed in the process of cleaning waste rock and residue by ecological restoration, and the leaching of arsenic alkali residue caused Sb containing wastewater to infiltrate into the groundwater environment and increase Sb content.

After ecological restoration, the correlations between Sb and TDS were higher than those before ecological restoration (Fig. 5f), and the TDS content also increased after ecological restoration (Table 1), indicating that the ecological restoration process strengthened the water-rock action in shallow groundwater. Strong water-rock interactions can promote the release of Sb from minerals.

Water-Rock Interaction Before and After Ecological Restoration

Groundwater chemistry is primarily affected by three natural mechanisms: atmospheric precipitation, rock weathering, and evaporation/concentration [40-43]. The relationships between Na⁺/(Na⁺+Ca²⁺) for cations, Cl⁻/(Cl⁻+HCO₃⁻) for anions, and TDS were analyzed to determine the dominant factors affecting the water composition (Fig. 7). In the Gibbs diagram, the upper-right corner represents the dominant field of the evaporation/concentration effect, the TDS value is higher, and the ratio of cations to cations is approximately unity. The atmospheric precipitation dominant field is located at the lower right, the TDS value is low, and the ratio of cations to cations is greater than 0.5. The dominant rock weathering field is at the left center of the diagram, the TDS value is at a moderate level, and the ratio of cations to cations is less than 0.5. As shown in Fig. 7, the shallow groundwater samples before ecological restoration fell between the

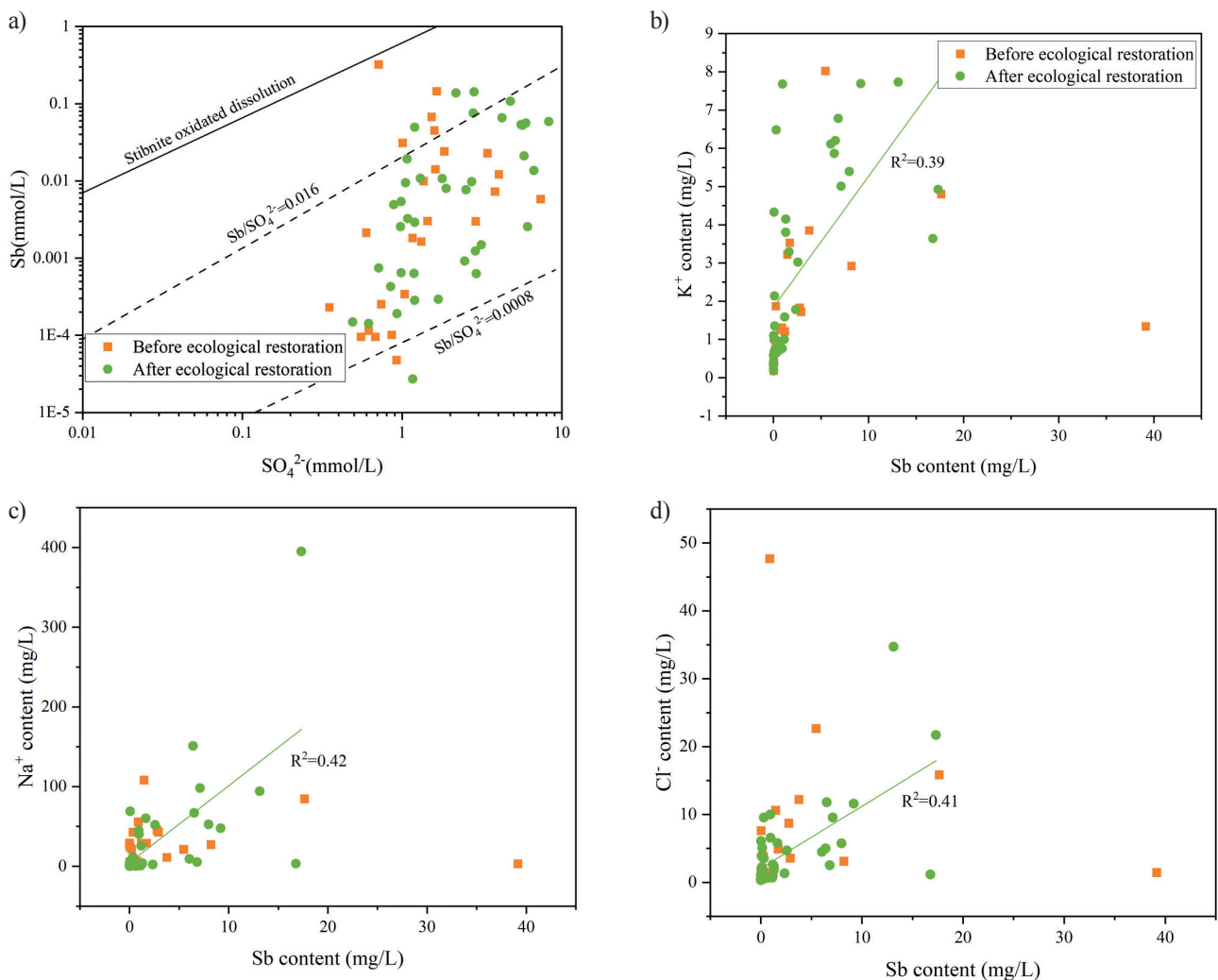


Fig. 5. Relationships between Sb content and the geochemical characteristics of groundwater samples: a) Sb versus SO₄²⁻; b) Sb versus K⁺; c) Sb versus Na⁺; d) Sb versus Cl⁻.

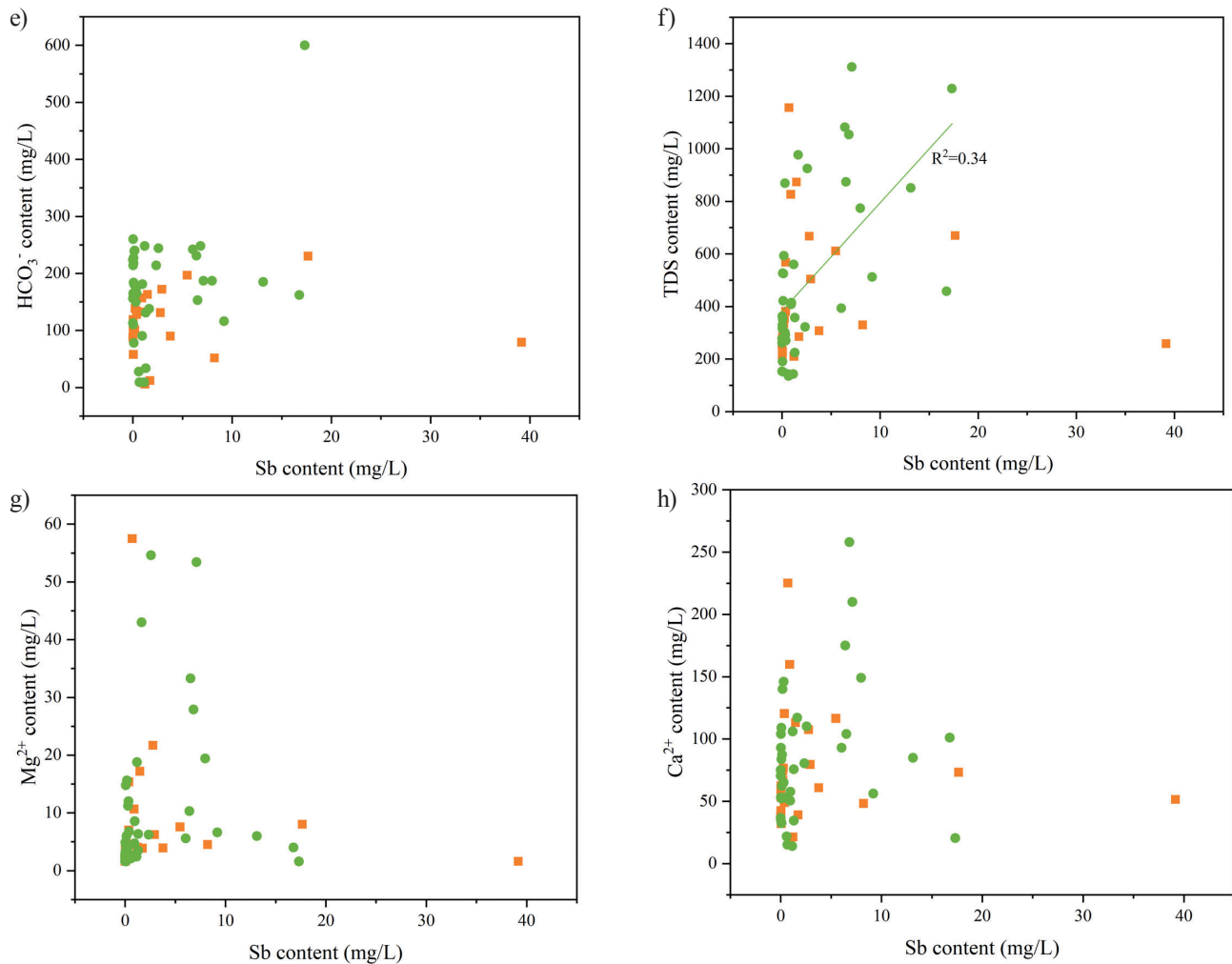


Fig. 5. Continued.

dominant fields of rock weathering and evaporation/concentration, indicating that the water-rock interactions of the shallow groundwater before ecological restoration

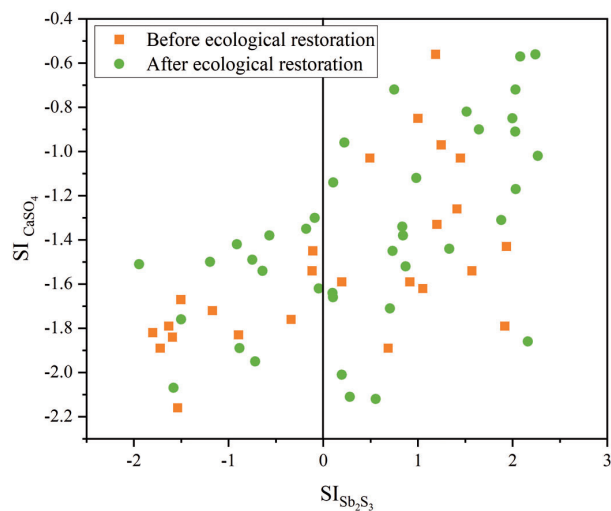


Fig. 6. Plots of the SI of stibnite versus the SI of gypsum.

were controlled by rock weathering and evaporation/concentration processes. Approximately 69.23% of the shallow groundwater samples after ecological restoration were located in the dominant field of rock weathering, indicating that the water-rock interaction after ecological restoration was mainly affected by rock weathering, which was consistent with the results of Hao et al. [36]. Water samples also appeared outside the Gibbs diagram, which can be attributed to anthropogenic pollution [44-46].

The ions produced by weathering of different rocks also differ. The influence of the weathering dissolution of evaporative, carbonate, and silicate rocks on the chemical components of water can be qualitatively determined by Na normalization [47, 48]. As shown in Fig. 8, the sample points before ecological restoration were mainly located in silicate weathering fields, and approximately 56% of the shallow groundwater samples were located between silicate mineral weathering and carbonate mineral weathering fields, suggesting that shallow groundwater was mainly affected by the water-rock interaction of silicate and carbonate minerals before ecological restoration. After ecological restoration,

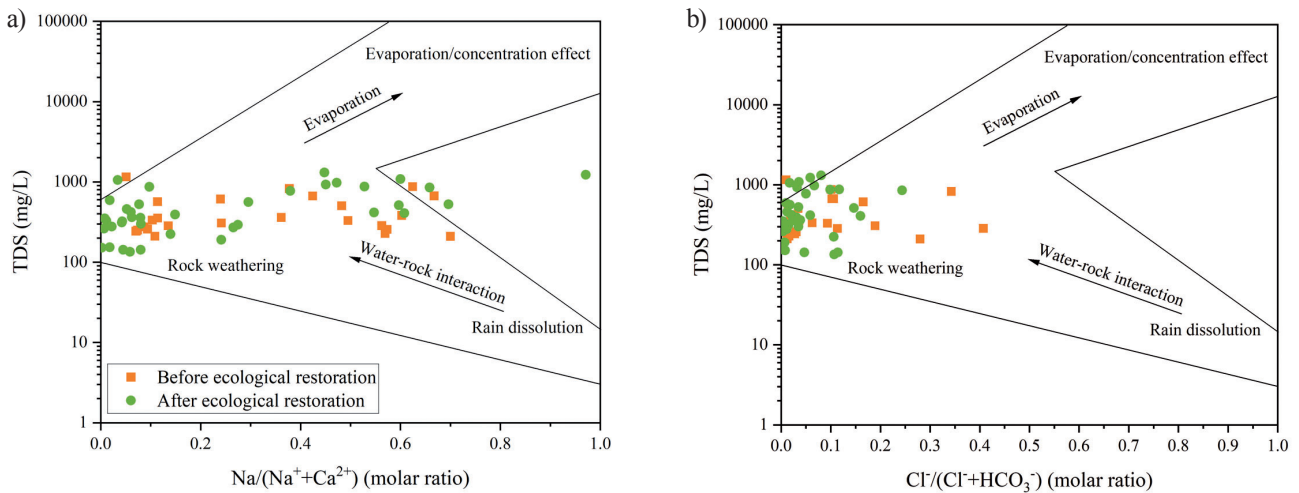


Fig. 7. Gibbs diagram of shallow groundwater samples in the study area..

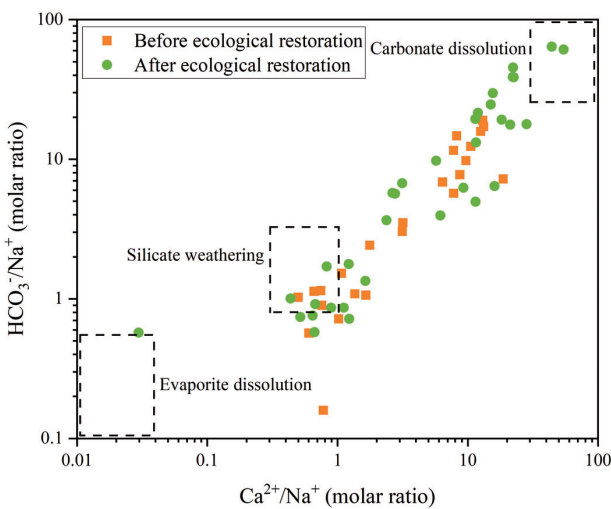


Fig. 8. Relationship between $[HCO_3^-]$ and $[Ca^{2+}]$ normalized by $[Na^+]$.

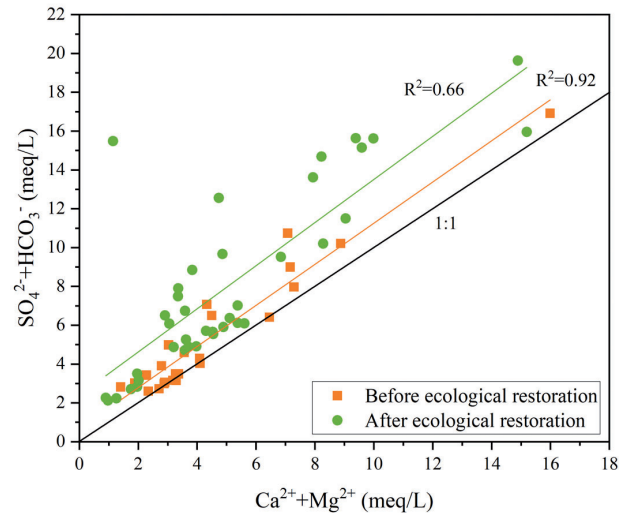
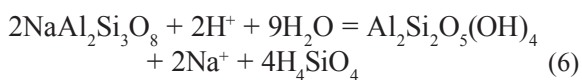


Fig. 9. Relation between $(Ca^{2+}+Mg^{2+})$ and $(SO_4^{2-}+HCO_3^-)$ of shallow groundwater samples.

approximately 28.20% of the sample points were located in a silicate weathering field, 2.56% were close to the dissolution of evaporative salt rock, and the sample points showed a trend towards carbonate dissolution. The results showed that the hydrogeochemical processes in the study area after ecological restoration were affected by weathering and hydrolysis of silicate minerals (such as albite), but the contribution of carbonate minerals cannot be excluded [43]. The water-rock reaction for albite ($NaAl_2Si_3O_8$) is as follows:



If Ca^{2+} , Mg^{2+} , SO_4^{2-} , and HCO_3^- are all derived from the dissolution of carbonate minerals, the milligram equivalent concentration ratio between $(Ca^{2+}+Mg^{2+})$ and $(HCO_3^-+SO_4^{2-})$ should be 1:1 [18, 49]. The deviation

between the water sample and the 1:1 dissolution line suggests that there are other water-rock interactions; the farther the water sample deviates from the dissolution line, the stronger the interactions between the other water rocks [50]. Before ecological restoration, approximately 72% of the sample points were above the dissolution line 1:1, and after ecological restoration, all sample points were located to the upper left of the dissolution line (Fig. 9). The correlation between $(Ca^{2+}+Mg^{2+})$ and $(HCO_3^-+SO_4^{2-})$ before ecological restoration ($R^2=0.92$) was higher than that after ecological restoration ($R^2=0.66$). The results indicate that the chemical composition of the shallow groundwater before ecological restoration was controlled by the dissolution of carbonate and silicate minerals, whereas the chemical composition of the shallow groundwater after ecological restoration was mainly controlled by the weathering and hydrolysis of silicate minerals.

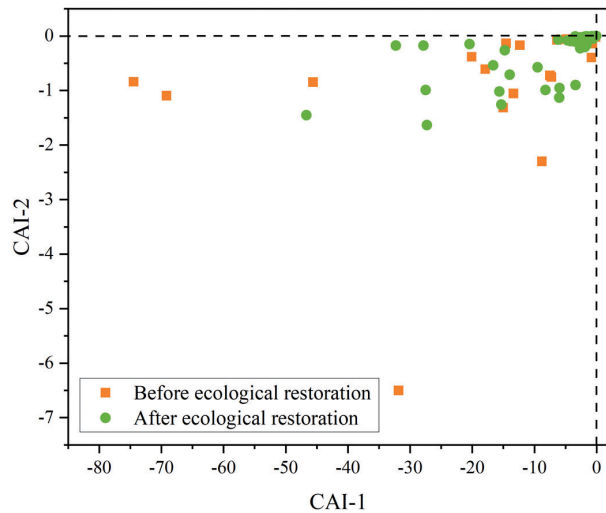


Fig. 10. CAI-1 vs. CAI-2 in shallow groundwater samples.

Ion-Exchange Interaction Before and After Ecological Restoration

Most scholars have adopted the chlor-alkali index (CAI-1 and CAI-2) proposed by Schoeller to clarify the effect of ion exchange on the chemical composition of groundwater [37, 51]. The two main factors CAI-1 and CAI-2 are expressed as follows:

$$\text{CAI-1} = [\text{Cl}^- - (\text{Na}^+ + \text{K}^+)] / \text{Cl}^- \quad (7)$$

$$\text{CAI-2} = [\text{Cl}^- - (\text{Na}^+ + \text{K}^+)] / (\text{HCO}_3^- + \text{CO}_3^{2-} + \text{NO}_3^-) \quad (8)$$

Positive values for the two indices indicate that Na^+ and K^+ ions in the groundwater displaced Ca^{2+} and Mg^{2+} in the aquifer, and cation exchange occurred. Conversely, reverse cation exchange occurred, and Ca^{2+} and Mg^{2+} in the groundwater were replaced by Na^+ and K^+ . The larger the absolute values of CAI-1 and CAI-2, the stronger is the alternating cation adsorption [37, 49]. In this study, all samples showed negative CAI-1 and CAI-2 values before and after ecological restoration (Fig. 10), indicating that Ca^{2+} and Mg^{2+} in the shallow groundwater were exchanged for Na^+ in the surrounding aquifer material. The Ca^{2+} content decreased, and the content of Na^+ increased after ecological restoration because of the effect of reverse ion exchange (Table 1). The CAI-1 and CAI-2 values of the shallow groundwater samples before ecological restoration were widely distributed, and their absolute values were greater than those after ecological restoration. Meanwhile, the Sb content after ecological restoration was lower than that before ecological restoration (Table 1), indicating that the cation exchange effect before ecological restoration was stronger than that after ecological restoration, and that the strong cation exchange interaction promoted the release of Sb, which was consistent with the results of Sun et al. [52].

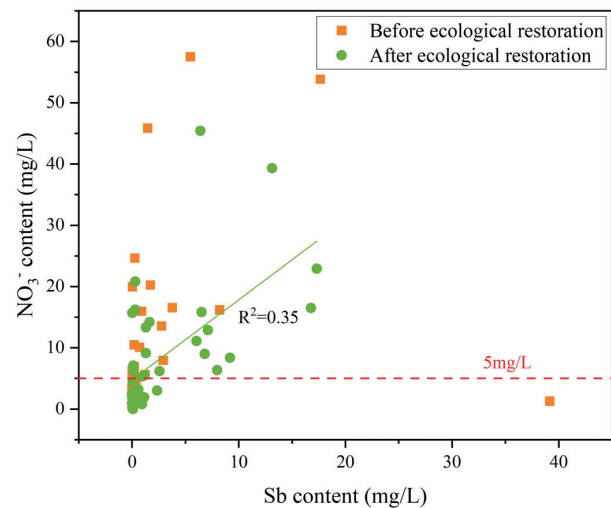


Fig. 11. Plots illustrating Sb vs. NO_3^- concentrations in shallow groundwater samples.

Agricultural Activities Before and After Ecological Restoration

The content of nitrate (NO_3^-) in the groundwater exceeds 5.00 mg/L, indicating that the groundwater environment was affected by agricultural activities [53, 54]. All water chemical samples before the ecological restoration and some water chemical samples after the ecological restoration were higher than the NO_3^- pollution limit (Fig. 11), suggesting that agricultural activities would affect the increase in Sb content. There was a positive correlation between Sb and NO_3^- after ecological restoration ($R^2 = 0.35$); therefore, the increase in Sb content caused by agricultural activities after ecological restoration can not be ignored. The ecological restoration project reclaims land in mining areas. The use of nitrogen-containing fertilizers, such as livestock manure, in the planting process, to a certain extent, causes nitrogen to infiltrate shallow groundwater along with atmospheric precipitation and agricultural irrigation, resulting in increased nitrogen content and Sb pollution.

Despite Sb content decreased in shallow groundwater after ecological restoration project in the study area, the majority of residents are not aware of the risks of Sb (III) from drinking, due to oxidization-reduction processes. These our findings are limited for assisting the informed management of groundwater resources for drinking within and analyzing Sb valence evolution before and after ecological restoration project in the study area.

Conclusions

To understand the hydrogeochemical factors and water-rock interaction mechanisms of Sb content changes before and after ecological restoration, hydrogeochemical data from 2011 to 2020 were

collected and analyzed. The main conclusions are as follows.

Before and after ecological restoration, the range of Sb concentrations in shallow groundwater was 0.006–39.160 mg/L (mean 3.501 mg/L) and 0.003–17.326 mg/L (mean 2.931 mg/L), respectively. The average Sb content after ecological restoration decreased 0.16 times compared to that before ecological restoration. The main hydrochemical types converted from Ca-Na-SO₄-HCO₃ (36.00%), Ca-HCO₃-SO₄ (32.00%), and Ca-SO₄-HCO₃ (16.00%) to Ca-HCO₃-SO₄ (33.33%), Ca-SO₄-HCO₃ (33.33%), and Ca-Na-SO₄-HCO₃ (12.82%) during ecological restoration.

Before ecological restoration, the high Sb groundwater environment was mainly affected by the oxidative dissolution of Sb₂S₃, weathering of carbonate and silicate minerals, the evaporation/concentration effect, and strong cation exchange. After ecological restoration, the treatment of Sb-related enterprises and cleaning of arsenic alkali residue achieved good results. Meanwhile, the dissolution of CaSO₄ inhibited the dissolution of Sb₂S₃ and reduced the Sb content.

By comprehensively analyzing the changes in hydrogeochemical ions and Sb content before and after ecological restoration, enhancing the understanding on the formation mechanism of high Sb concentrations in shallow groundwater in the study area can be understood. Overall, it is highly suggested all the parts of geochemical cycle to find the mobilization pathways, oxidation-reduction mechanisms and health risk of Sb after ecological restoration project should be taken in the future in efforts to improve public safety. The findings of this study provide a comprehensive assessment of the influence of the ecological restoration project on the Sb content evolution in shallow groundwater quality and ensure the drinking water safety in the study area.

Acknowledgments

This work was supported by the Natural Science Foundation of Hebei Province (D2021508004), Research Foundation of the Department of Natural Resources of Hunan Province (20230150ST) and the ecological restoration project in the Lengshuijiang antimony mine area (Grant LCG2020009).

Conflict of Interest

The authors declare no conflict of interest.

References

- LIU F., LE X.C., MCKNIGHT-WHITFORD A., XIA Y.L., WU F.C., ELSWICK E., JOHNSON C.C., ZHU C. Antimony speciation and contamination of waters in the

- Xikuangshan antimony mining and smelting area, China. *Environmental Geochemistry and Health*, **32** (5), 401, **2010**.
- WEN B., ZHOU J.W., ZHOU A.G., LIU C.F., XIE L. Sources, migration and transformation of antimony contamination in the water environment of Xikuangshan, China: Evidence from geochemical and stable isotope (S, Sr) signatures. *Science of the Total Environment*, **569–570**, 114, **2016**.
- BOREIKO C.J., ROSSMAN T.G. Antimony and its compounds: Health impacts related to pulmonary toxicity, cancer, and genotoxicity. *Toxicology and Applied Pharmacology*, **403**, **2020**.
- GU W., PANG R.F., CHEN Y.Y., DENG F.C., ZHANG M., SHAO Z.J., ZHANG S.Y., DUAN H.W., TANG S. Short-term exposure to antimony induces hepatotoxicity and metabolic remodeling in rats. *Ecotoxicology and Environmental Safety*, **256**, 114852, **2023**.
- LAI Z.Y., HE M.C., LIN C.Y., OUYANG W., LIU X. Interactions of antimony with biomolecules and its effects on human health. *Ecotoxicology and Environmental Safety*, **233**, 113317, **2022**.
- CAVALLO D., IAVICOLI I., SETINI A., MARINACCIO A., PERNICONI B., CARELLI G., IAVICOLI S. Genotoxic risk and oxidative DNA damage in workers exposed to antimony trioxide. *Environmental and Molecular Mutagenesis*, **40** (3), 184, **2002**.
- CIDU R., BIDDAU R., DORE E., VACCA A., MARINI L. Antimony in the soil-water-plant system at the Su Suergiu abandoned mine (Sardinia, Italy): strategies to mitigate contamination. *Science of the Total Environment*, **497–498**, 319, **2014**.
- ASHLEY P.M., CRAW D., GRAHAM B.P., CHAPPELL D.A. Environmental mobility of antimony around mesothermal stibnite deposits, New South Wales, Australia and southern New Zealand. *Journal of Geochemical Exploration*, **77** (1), 1, **2003**.
- FU Z.Y., WU F.C., MO C.L., DENG Q.J., MENG W., GIESY J.P. Comparison of arsenic and antimony biogeochemical behavior in water, soil and tailings from Xikuangshan, China. *Science of the Total Environment*, **539**, 97, **2016**.
- PALMER M.J., CHETELAT J., RICHARDSON M., JAMIESON H.E., GALLOWAY J.M. Seasonal variation of arsenic and antimony in surface waters of small subarctic lakes impacted by legacy mining pollution near Yellowknife, NT, Canada. *Science of the Total Environment*, **684**, 326, **2019**.
- NYAKUNDI R., NYADAWA M., MWANGI J. Effect of Recharge and Abstraction on Groundwater Levels. *Civil Engineering Journal*, **8** (5), 910, **2022**.
- JOHNSTON S.G., BENNETT W.W., DORIEAN N., HOCKMANN K., KARIMIAN N., BURTON E.D. Antimony and arsenic speciation, redox-cycling and contrasting mobility in a mining-impacted river system. *Science of the Total Environment*, **710**, 136354, **2020**.
- LIANG Y.P., GAO X.B., ZHAO C.H., TANG C.L., SHEN H.Y., WANG Z.H., WANG Y.X. Review: Characterization, evolution, and environmental issues of karst water systems in Northern China. *Hydrogeology Journal*, **26** (5), 1371, **2018**.
- LI X.Q., PAN G.F., ZHOU A.G., FANG L., HE N.J. Stable sulfur and oxygen isotopes of sulfate as tracers of antimony and arsenic pollution sources related to antimony mine activities in an impacted river. *Applied Geochemistry*, **142**, **2022**.

15. NGUYEN T.G., PHAN K.A., HUYNH T.H.N. Application of Integrated-Weight Water Quality Index in Groundwater Quality Evaluation. *Civil Engineering Journal*. **8** (11), 2661, **2022**.
16. FILELLA M., BELZILE N., CHEN Y.-W. Antimony in the environment: a review focused on natural waters I. Occurrence. *Earth-Science Reviews*, **57** (1-2), 125, **2002**.
17. HE M.C., WANG X.Q., WU F.C., FU Z.Y. Antimony pollution in China. *Science of the Total Environment*, **421-422**, 41, **2012**.
18. FANG L., ZHOU A.G., LI X.Q., ZHOU J.W., PAN G.F., HE N.J. Response of antimony and arsenic in karst aquifers and groundwater geochemistry to the influence of mine activities at the world's largest antimony mine, central China. *Journal of Hydrology*, **603**, **2021**.
19. HE M.C., WANG N.N., LONG X.J., ZHANG C.J., MA C.L., ZHONG Q.Y., WANG A.H., WANG Y., PERVAIZ A., SHAN J. Antimony speciation in the environment: Recent advances in understanding the biogeochemical processes and ecological effects. *Journal of Environmental Sciences*, **75**, 14, **2019**.
20. SCHÖPKE, R., WALKO, M. Control of the Remediation of Anoxic AMD Groundwater by Sulphate Reduction in a Subsoil Reactor. *Journal of Human, Earth, and Future*. **3** (3), 280, **2022**.
21. CIDU R., BIDDAU R., DORE E., VACCA A. Antimony Dispersion at Abandoned Mines in Sardinia, Italy. *Procedia Earth and Planetary Science*, **7**, 171, **2013**.
22. NING Z.P., XIAO T.F., YANG F., JIA Y.L., SUN J.L., HE L.B. Antimony pollution and sulfur isotope study in the waters of an antimony mine area. *Bulletin of Mineralogy, Petrology and Geochemistry*, **30** (2), 135, **2011**.
23. USGS Mineral Commodity Summaries 2020. U.S. Geological Survey, 22, **2020**.
24. ZHOU Y.L. Mineral Resources and Progress in Smelting and Extraction of Antimony. *Hunan Nonferrous Metals*, **38** (6), 39, **2022**.
25. GUO X.J., WANG K.P., HE M.C., LIU Z.W., YANG H.L., LI S.S. Antimony smelting process generating solid wastes and dust: characterization and leaching behaviors. *Journal of Environmental Sciences*, **26** (7), 1549, **2014**.
26. ZHU J., GUO J.Y., WANG L.Y., FU Z.Y., LIAO H.Q., PAN X.L., WU F.C. Overview on Research on Environmentally Geochemical Characteristics of Antimony. *Earth and Environment*, **J. 38** (1), 109, **2010**.
27. LI W.Y., ZHOU J.W., JIA X.C., TANG P.D. EEMs characteristics of dissolved organic matter in water environment and its implications for antimony contamination in antimony mine of Xikuangshan, Hunan Province. *Bulletin of Geological Science and Technology*, **41** (04), 215, **2022**.
28. FAN D.L., ZHANG T., YE J. The Xikuangshan Sb deposit hosted by the Upper Devonian black shale series, Hunan, China. *Ore Geology Reviews*, **24** (1-2), 121, **2004**.
29. ZHOU J.W., NYIRENDA M.T., XIE L., LI Y., ZHOU B.L., ZHU Y., LIU H.L. Mine waste acidic potential and distribution of antimony and arsenic in waters of the Xikuangshan mine, China. *Applied Geochemistry*, **77**, 52, **2017**.
30. WEN B., ZHOU J.W., JIA X.C., ZHOU W.Q., HUANG Y.L. Attenuation of antimony in groundwater from the Xikuangshan antimony mine, China: Evidence from sulfur and molybdenum isotope study. *Applied Geochemistry*, **146**, **2022**.
31. MCCLESKEY R.B., NORDSTROM D.K., MAEST A.S. Preservation of water samples for arsenic (III/V) determinations: an evaluation of the literature and new analytical results. *Applied Geochemistry*, **19** (7), 995, **2004**.
32. DAUS B., WENNRICH R. Investigation on stability and preservation of antimonite in iron rich water samples. *Analytica Chimica Acta*, **847**, 44, **2014**.
33. NYIRENDA T.M., ZHOU J., MAPOMA H.W.T., XIE L., LI Y. Hydrogeochemical characteristics of groundwater at the Xikuangshan antimony mine in south China. *Mine Water and the Environment*, **35** (1), 86, **2015**.
34. HU X.Y., HE M.C., LI S.S., GUO X.J. The leaching characteristics and changes in the leached layer of antimony-bearing ores from China. *Journal of Geochemical Exploration*, **176**, 76, **2017**.
35. GUO W.J., FU Z.Y., WANG H., SONG F.H., WU F.C., GIESY J. P. Environmental geochemical and spatial/temporal behavior of total and speciation of antimony in typical contaminated aquatic environment from Xikuangshan, China. *Microchemical Journal*. **137**, 181, **2018**.
36. HAO C.M., LIU M., PENG Y.G., WEI Z. Comparison of Antimony Sources and Hydrogeochemical Processes in Shallow and Deep Groundwater Near the Xikuangshan Mine, Hunan Province, China. *Mine Water and the Environment*, **41** (1), 194, **2021**.
37. CHEN W.X., LIU P., LUO Y., LI B., PENG J.C., JIN X.J. Behavior of Sb and As in the hydrogeochemistry of adjacent karst underground river systems and the responses of such systems to mining activities. *Science of the Total Environment*, **857** (Pt 1), 159411, **2023**.
38. LONG H., ZHENG Y.-J., PENG Y.-L., HE H.-B. Recovery of alkali, selenium and arsenic from antimony smelting arsenic-alkali residue. *Journal of Cleaner Production*, **251**, **2020**.
39. DENG W.H., CHAI L.Y., DAI Y.J. Industrial experimental study on comprehensive recovering valuable resources from antimony smelting arsenic alkali residue. *Hunan Nonferrous Metals*, **30** (3), 24, **2014**.
40. GIBBS R.J. Mechanisms Controlling World Water Chemistry. *Science*, **170** (3962), **1970**.
41. WU C., WU X., QIAN C., ZHU G. Hydrogeochemistry and groundwater quality assessment of high fluoride levels in the Yanchi endorheic region, northwest China. *Applied Geochemistry*, **98**, 404, **2018**.
42. LI Z.J., YANG Q.C., YANG Y.S., MA H.Y., WANG H., LUO J.N., BIAN J.M., MARTIN J.D. Isotopic and geochemical interpretation of groundwater under the influences of anthropogenic activities. *Journal of Hydrology*, **576**, 685, **2019**.
43. HAO C.M., ZHANG W., GUI H.R. Hydrogeochemistry characteristic contrasts between low- and high-antimony in shallow drinkable groundwater at the largest antimony mine in hunan province, China. *Applied Geochemistry*, **117**, **2020**.
44. PU J.B., YUAN D.X., JIANG Y.J., GOU P.F., YIN J.J. Hydrogeochemistry and environmental meaning of Chongqing subterranean karst streams in China. *Advances in Water Science*, **J. 21** (5), 628, **2010**.
45. MATTOS J.B., CRUZ M.J.M., DE PAULA F.C.F., SALES E.F. Spatio-seasonal changes in the hydrogeochemistry of groundwaters in a highland tropical zone. *Journal of South American Earth Sciences*, **88**, 275, **2018**.
46. SELVAKUMAR S., CHANDRASEKAR N., KUMAR G. Hydrogeochemical characteristics and groundwater contamination in the rapid urban development areas of

- Coimbatore, India. *Water Resources and Industry*, **17**, 26, **2017**.
47. JIANG L.G., YAO Z.J., LIU Z.F., WANG R., WU S.S. Hydrochemistry and its controlling factors of rivers in the source region of the Yangtze River on the Tibetan Plateau. *Journal of Geochemical Exploration*, **155**, 76, **2015**.
48. CHEN J.S., WANG F.Y., XIA X.H., ZHANG L.T. Major element chemistry of the Changjiang (Yangtze River). *Chemical Geology*, **187**, 231, **2002**.
49. KUMAR P., SINGH C.K., SARASWAT C., MISHRA B., SHARMA T. Evaluation of aqueous geochemistry of fluoride enriched groundwater: A case study of the Patan district, Gujarat, Western India. *Water Science*, **31** (2), 215, **2019**.
50. WALTER J., CHESNAUX R., CLOUTIER V., GABOURY D. The influence of water/rock – water/clay interactions and mixing in the salinization processes of groundwater. *Journal of Hydrology: Regional Studies*, **13**, 168, **2017**.
51. DE A., MRIDHA D., JOARDAR M., DAS A., CHOWDHURY N.R., ROYCHOWDHURY T. Distribution, prevalence and health risk assessment of fluoride and arsenic in groundwater from lower Gangetic plain in West Bengal, India. *Groundwater for Sustainable Development*, **16**, **2022**.
52. SUN X.M., LI Y., LIU C., ZHANG L., LI Z., HAO C.M. Morphological Distribution and Formation Mechanisms of Antimony in the Shallow Groundwater of the Xikuangshan Antimony Mine in Hunan, China. *Frontiers in Environmental Science*, **10**, **2022**.
53. LI D.N., GAO X.B., WANG Y.X., LUO W.T. Diverse mechanisms drive fluoride enrichment in groundwater in two neighboring sites in northern China. *Environmental Pollution*, **237**, 430, **2018**.
54. SU H., KANG W.D., LI Y.R., LI Z. Fluoride and nitrate contamination of groundwater in the Loess Plateau, China: Sources and related human health risks. *Environmental Pollution*, **286**, 117287, **2021**.